


## RESEARCH ARTICLE

# Bioactive nano-fibrous scaffold for vascularized craniofacial bone regeneration

Rahul Damodaran Prabha<sup>1,3,4</sup>  | David Christian Evar Kraft<sup>4</sup> | Linda Harkness<sup>1</sup> | Birte Melsen<sup>4</sup> | Harikrishna Varma<sup>2</sup> | Prabha D. Nair<sup>2</sup> | Jorgen Kjems<sup>3</sup> | Moustapha Kassem<sup>1</sup>

<sup>1</sup>Department of Endocrinology and Metabolism, University Hospital of Odense, Odense, Denmark

<sup>2</sup>Sree Chitra Tirunal Institute for Medical Sciences and Technology (SCTIMST), Thiruvananthapuram, Kerala, India

<sup>3</sup>Interdisciplinary Nanoscience Center (iNANO), Aarhus University, Aarhus, Denmark

<sup>4</sup>Section of Orthodontics, Department of Dentistry, Aarhus University, Aarhus, Denmark

## Correspondence

Rahul Damodaran Prabha, Department of Endocrinology and Metabolism, University Hospital of Odense, University of Southern Denmark, Winslowparken 25, 1st Floor, DK-5000 Odense C, Denmark.  
Email: rahuldp6@gmail.com

## Present Address

Rahul Damodaran Prabha, Department of Orthodontics and Dentofacial Orthopedics, Amrita School of Dentistry, Amrita University, Kochi, Kerala -682041, India.  
Email: rahuldp6@gmail.com

## Funding information

Lundbeck Foundation Nano medicine Center for Individualized Management of Tissue Damage and Regeneration; Indo-Danish grant obtained from The strategic research council of Denmark and Department of Biotechnology; India

## Abstract

There has been a growing demand for bone grafts for correction of bone defects in complicated fractures or tumours in the craniofacial region. Soft flexible membrane like material that could be inserted into defect by less invasive approaches; promote osteoconductivity and act as a barrier to soft tissue in growth while promoting bone formation is an attractive option for this region. Electrospinning has recently emerged as one of the most promising techniques for fabrication of extracellular matrix such as nano-fibrous scaffolds that can serve as a template for bone formation. To overcome the limitation of cell penetration of electrospun scaffolds and improve on its osteoconductive nature, in this study, we fabricated a novel electrospun composite scaffold of polyvinyl alcohol (PVA)-poly ( $\epsilon$ ) caprolactone (PCL)-Hydroxyapatite based bioceramic (HAB), namely, PVA-PCL-HAB. The scaffold prepared by dual electrospinning of PVA and PCL with HAB overcomes reduced cell attachment associated with hydrophobic PCL by combination with a hydrophilic PVA and the HAB can contribute to enhance osteoconductivity. We characterized the physicochemical and biocompatibility properties of the new scaffold material. Our results indicate PVA-PCL-HAB scaffolds support attachment and growth of stromal stem cells; [human bone marrow skeletal (mesenchymal) stem cells and dental pulp stem cells]. In addition, the scaffold supported *in vitro* osteogenic differentiation and *in vivo* vascularized bone formation. Thus, PVA-PCL-HAB scaffold is a suitable potential material for therapeutic bone regeneration in dentistry and orthopaedics.

## KEYWORDS

bioceramics, bone, craniofacial, electrospinning, scaffold, stem cells

## 1 | INTRODUCTION

Over the past few decades, there has been a growing demand for bone grafting for correcting bone defects in complicated fractures, following tumour resection or during repair of developmental disorders-associated pathologies in the craniofacial region (Giannoudis, Dinopoulos, & Tsiridis, 2005). Traditionally, autologous bone tissue has been the gold standard for bone grafting. However, donor site morbidity, inadequate supply, and other associated impediments have encouraged search for alternative sources of bone (Giannoudis et al., 2005). A promising alternative source is tissue-engineered

bone derived from interaction of stromal skeletal (mesenchymal) stem cells (MSCs), biomaterial scaffolds, and growth factors (Mikos et al., 2006). To be clinically useful, the properties of tissue-engineered bone should “mimic” the native bone tissue (Mikos et al., 2006).

A large number of scaffolds with a wide number of applications ranging from mere bone filler to more specialized scaffolds have been developed for bone tissue engineering (Kouroupis, Baboolal, Jones, & Giannoudis, 2013; Wu, Zhou, Chang, & Xiao, 2013; Yang, Wang, Hou, Guo, & Liu, 2013). The scaffolds should provide a supporting surface for MSCs and in addition, they are expected to be biocompatible and

bioactive (osteoconductive, allowing bone cells to grow on or osteoinductive, inducing new bone formation) as well as biodegradable at the rate of new bone formation (Jones, 2013). The scaffolds are also expected to exhibit these ideal properties consistently when fabricated on a large scale, following sterilization and when used clinically (Jones, 2013). The craniofacial region contains bones of varying shape, density, and morphology and accommodates many vital organs and tissues. The healing of critical bone defects is better with patent vascular supply (Garcia & Garcia, 2015) and inhibited by adjacent soft tissue.

Scaffolds that are soft flexible membrane like material that could be inserted into defect by less invasive approaches, promote osteoconductivity, and act as a barrier to soft tissue in growth while promoting bone formation is an attractive option for this region. Electrospinning has recently emerged as one of the most promising techniques for fabrication of soft and extracellular matrix such as nano-fibrous scaffolds that can serve as a template for bone formation. Numerous polymers and natural tissue derivatives have been employed to fabricate scaffolds suitable for use in bone tissues. poly ( $\epsilon$ ) caprolactone (PCL) is widely chosen for its biocompatibility and mechanical properties (Ciapetti et al., 2003). However, PCL exhibit hydrophobicity, which leads to limited cell attachment and also delayed biodegradation (Mohan & Nair, 2008). Hydrophobicity of PCL tends to prevent cell migration and prolongs scaffold integration with host tissue (Zhu, Gao, Liu, & Shen, 2002). One promising method of reducing hydrophobicity and increasing porosity of PCL is dual electrospinning of PCL with a hydrophilic and biocompatible polymer, for example, polyvinyl alcohol (PVA). PVA also introduces several free hydroxyl chains, which can be employed for scaffold functionalization via linking drugs, biomolecules, or growth factors (Orienti, Bigucci, Gentilomi, & Zecchi, 2001). The electrospun composite of PVA and PCL is food and drug administration-approved biomaterial for clinical use. The electrospun PVA-PCL material may be combined with a bioactive bioceramic for improving on osteoconductivity.

Hydroxyapatite based Bioceramic (HAB) is triphasic bioceramic developed by incorporation of hydroxyapatite, beta tricalcium phosphate, calcium silicates, and traces of magnesium in a unique combination to act synergistically to produce an osteoconductive and osteoinductive material (Jones, 2013). Magnesium was incorporated to aid in improve sintering window as well as to generate osteoimmunomodulatory effect (Chen et al., 2014). Incorporation of silicates facilitates bioactivity of scaffold and subsequent vascularization of the scaffold construct (Gorustovich, Roether, & Boccaccini, 2010). It is plausible that PVA and PCL along with an osteoconductive material such as bioactive HAB triphasic bioceramic is an ideal material suitable for craniofacial bone tissue engineering.

To investigate the application of the scaffold for bone regeneration, we tested with the stromal cells, namely, human bone marrow skeletal (mesenchymal) stem cells (hMSC) and dental pulp stem cells (DPSC) in vitro. The hMSC are bone marrow derived skeletal stem cells and widely reported to differentiate into osteoblast upon induction. We also tested DPSC, cells of craniofacial region; to understand possible interaction of cells of neural crest origin on the scaffold. Both the cells served as biological replicates to test wider application of scaffold for bone regeneration in the skeletal system

The present study hence aims to fabricate a novel electrospun composite scaffold PVA-PCL-HAB, with nano-fibrous structure and osteoconductive nature, and to investigate its potential role in bone regeneration by combining with bone marrow-derived MSCs or DPSC through in vitro and in vivo studies in mice models

## 2 | MATERIALS AND METHODS

### 2.1 | Scaffold fabrication and physicochemical characterization

#### 2.1.1 | Bioceramic (HAB) fabrication

HAB was prepared by refluxing a solution of tetraethyl-orthosilicate (Sigma-Aldrich, Germany) in ethanol (Sigma Gmbh, Germany). Calcium nitrate (Rankem, India), calcium fluoride (SD Fine, India), and magnesium nitrate (SD Fine, India) dissolved in orthophosphoric acid (SD Fine, India) was added to the refluxed tetraethyl-orthosilicate solution with heating. The mixture was heated and allowed to undergo gelation. The gel formed was dried and calcinated in a raising-hearth electric furnace (Bysakh & Co, India) at 600 °C for 3 hr. The product was then compacted and sintered at 1,200 °C for 2 hr. The obtained product was then milled in a planetary ball mill (Retsch, Germany) at 250 rpm for 20 min. The HAB powder, where then sieved through 20  $\mu$ m sieve (Retsch, Germany).

#### 2.1.2 | Electrospinning

Ten percent w/v PCL solution (70,000–90,000 Mw, Sigma-Aldrich, USA) was prepared in a mixture of chloroform and methanol (70:30). 10% w/v PVA (89,000–98,000 Mw, Sigma Aldrich, USA) solution was prepared by addition of PVA into boiling distilled water. The 0.5% w/v bioceramic granules were then dispersed in PCL solution by sonication. The electrospinning of scaffolds were performed in a commercially available unit (Holmarc Nanofiber spinning station, India). The dual electrospinning technique employed was with a dual pump and dual syringe system. The spinning parameters are described in (Table S1). The electrospun PVA-PCL-HAB obtained were then cross-linked by glutaraldehyde (Sigma Aldrich, USA) solution prepared in 70% isopropyl alcohol (SD-Fine chemical limited, India) with conc. hydrochloric acid (SD-Fine chemical limited, India) added to the cross-linking solution as a catalyst. The cross linked product was washed in 50% isopropanol and further in water to remove unreacted components. The PVA-PCL-HAB scaffold obtained was then air dried in a laminar flow hood. The morphology of scaffold was imaged with scanning electron microscopy [SEM] (Nova NanoSEM 600; FEI Company, Netherlands and Hitachi S 2400, Japan).

#### 2.1.3 | Physicochemical characterization

The chemical compositions of the scaffolds were ascertained by comparing the Fourier transform infrared with attenuated total reflectance (FTIR-ATR) spectra of scaffold and its individual components. FTIR-ATR spectra was obtained using ThermoNicolet 5700 FTIR with diamond ATR accessory, in the frequency range of (4,000–400  $\text{cm}^{-1}$ ). The thermal stability of the samples was determined by thermogravimetric analysis as according to ASTM E1131-03 using

thermogravimetric analysis (TGA)-differential thermal analysis instrument (Model SDT 2920 TA Instruments Inc., New Castle, DE).

Water contact angle testing and swelling studies was performed to quantify the hydroaffinity of the scaffolds. The sessile drop method was employed to record water-in-air contact angles of the scaffolds at room temperature (25 °C) using a video-based contact angle measuring device (Data Physics OCA15 plus) and imaging software (SCA 20 software) our published protocol (Thomas & Nair, 2011).

For the swelling studies, electrospun PVA, electrospun PCL, and PVA-PCL-HAB were cut into squares of 100 mm<sup>2</sup> sizes, weighed, and immersed in distilled water (pH 7.4) for continuous intervals of time. The strips were removed and carefully blotted using filter paper to remove excess fluid and weighed. The swelling index calculated by the formula = ((Final weight-Initial weight) / (Initial weight)) × 100

### 2.1.4 | Ion washout

PVA-PCL-HAB was cut into 1 cm<sup>2</sup> area were immersed in 1 ml of phosphate buffered saline (PBS) at 37 °C with pH of 7.4. Total volumes of the PBS were replaced with fresh PBS at Day 1, 3, 5, 7, and 14 (Andersen et al., 2013). Ionic concentration of calcium ions and silica ions released into the washout PBS was quantified with inductive coupled plasma optical emission spectroscopy (ICP-OES) (5300DV, Perkin Elmer, USA).

### 2.1.5 | Stimulated body fluid immersion

Stimulated body fluid (SBF) immersion experiment was performed to test the in vitro apatite forming ability of the scaffold (Kokubo & Takadama, 2006). The scaffolds of 7 mm<sup>2</sup> area were immersed in 10 ml SBF (pH 7.4) and incubated at 37 °C for 30 days. The samples collected at Days 14 and 30, were washed with deionized water and dried at 37 °C. The apatite formation on the PVA-PCL-HAB were imaged by SEM and analysed by energy dispersive x-ray spectroscopy (EDAX).

## 2.2 | Cell culture

### 2.2.1 | Cell isolation and characterization

The DPSC were obtained from therapeutically extracted fully developed impacted healthy third molars from healthy young adult donors. The procedure was performed in accordance with the approved guidelines of The Central Denmark Region Committee on Biomedical Research Ethics. The isolation of DPSC, preparation of culture medium (CM), and osteogenic induction medium (OB) were performed as previously described (Kraft et al., 2010). For bone marrow MSCs, we used the human telomerase immortalized bone marrow derived skeletal stem cell line: hMSC-TERT that has been created in our laboratory and expresses all markers characteristics of primary hMSC including in vivo bone formation (Al-Nbaheen et al., 2013; Simonsen et al., 2002). For simplicity, we will refer to these cells hereafter as hMSC. All experiments included have a control group supplemented with CM and an osteogenic differentiation group supplemented with OB.

### 2.2.2 | MSCs characterization

Flow cytometry was performed on the cells to evaluate the MSC surface marker expression. DPSC and hMSC, were separately trypsinized to a single cell suspension, were blocked in 2% bovine serum albumin before incubation with pre-conjugated antibodies, or matched isotype controls (Table S3), for 45 min on ice. All samples were washed in FACS buffer (PBS, 40 nM EDTA, and FBS 2%) and were analysed with Beckman Coulter Cell Lab Quanta™ SC and WinMdi software.

### 2.2.3 | Cell seeding, attachment, spreading, and proliferation

The PVA-PCL-HAB scaffolds of 3 mm diameter were punched out using biopsy punch (Kai Europe GmbH, Germany). Scaffolds were sterilized in 70% ethanol for 30 min, followed by washing thrice in sterile water and further sterilized by dried under UV light (Rainer et al., 2010) for 30 min. Prior to seeding, the scaffolds were conditioned by wetting with culture media to obtain uniform seeding. The conditioned scaffolds placed in ultralow adhesion tissue culture plates (Costar, Corning) were seeded with 3 × 10<sup>4</sup> cells in 5 µl per scaffold. Scaffolds were then incubated at 37 °C, 5% CO<sub>2</sub> for 45 min to allow cell attachment. The CM was supplemented immediately after the cell attachment. Osteogenic induction was initiated at 24 hr, postseeding.

Cell attachment and proliferation on the PVA-PCL-HAB were assessed by DAPI/Phalloidin staining and Cell Titre-Blue (Promega, Madison, USA) assay, respectively, for time points 1, 2, 5, and 7 days. DAPI/ Phalloidin staining were performed as per, protocol (Andersen et al., 2013). The stained PVA-PCL-HAB were imaged under Olympus FV1000MPE Confocal microscope for DAPI (359 nm) and Phalloidin (550 nm), respectively.

Cell spreading on scaffolds were examined by SEM. PVA-PCL-HAB seeded with lower cell density 1,000 cells/scaffolds were fixed in 2.5% glutaraldehyde for 1 hr, washed in PBS, and dehydrated in graded series of alcohol and SEM performed at conditions stated previously (Shabani, Haddadi-Asl, Soleimani, Seyedjafari, & Hashemi, 2014). The spreading of cells on scaffolds was imaged at 1, 5, 10, and 15 days. The proliferation of cells seeded on the scaffolds was estimated by number of viable cells using Cell Titre-Blue reagent (Promega, Madison, USA). The absorbance measured was normalized to the standard linear curve established to obtain cell number. The assumption made was cells are not metabolically active until 24 hr.

### 2.2.4 | ALP activity

Alkaline phosphatase (ALP) activity was measured by using enzymatic *p*-nitrophenyl phosphate (Sigma-Aldrich) substrate reduction and further, normalized against the cell number. Cell number was quantified by the addition of Cell Titre-Blue reagent to culture medium, incubating at 37 °C for 1 hr, and measuring fluorescent intensity (560<sub>EX</sub>/590<sub>EM</sub>). Samples were then washed with PBS and Tris-buffered saline, fixed with 3.7% formaldehyde in 90% ethanol for 30 s at room temperature, incubated with substrate (1 mg/ml of *p*-nitro phenyl phosphate in 50 mM NaHCO<sub>3</sub>, pH 9.6, and 1 mM MgCl<sub>2</sub>) at 37 °C for 20 min,

and the absorbance measured at 405 nm (Qiu et al., 2010). ALP activity was normalized to cell number. ALP activity of cells on tissue culture plates (Plastic) with CM and OB were used as positive controls.

### 2.2.5 | Cytochemical staining

ALP staining (Harkness et al., 2011) and Alizarin red staining (AZR; Harkness et al., 2011); (Sigma-Aldrich, Denmark) for osteogenic differentiation was performed postfixation using either ice cold 70% ethanol for 1 hr (AZR) or 0.10 mM citrate buffer pH 4.2/acetone fix (ratio 3:2) for 5 min at room temperature (ALP). ALP staining was carried out with a (ratio 1:1) solution mix of 0.2 mg/ml Naphthol AS-TR phosphate substrate (Sigma-Aldrich, Denmark) in water and 0.417 mg/ml of Fast red (Sigma-Aldrich, Denmark) in 0.1 M Tris (pH 9.5) for 1 hr at room temperature. Samples for AZR staining were incubated in 40 mM AZR at pH 4.2 for 10 min at room temperature followed by washing in distilled water and PBS, before examination for the presence of mineralized matrix.

### 2.2.6 | Osteogenic gene expression

Cell seeded on PVA-PCL-HAB and the controls, cells seeded on culture plates (Plastic) were lysed for total RNA extraction using Trizol (Invitrogen, Denmark); according to manufacturer's instructions, the RNA pellets obtained were quantified using NanoDrop1000 spectrophotometer v3.7 instrument (Thermo Fisher Scientific, U. S. A). cDNA were constructed using a revertAid H minus first strand cDNA synthesis kit (Fermentas, St Leon-Rot, Germany) according to the manufacturer's instructions. RT-qPCR analysis was performed with StepOnePlus™ system (Applied Biosystems, Denmark). Following normalization to reference genes, quantification of relative gene expression was carried out using a comparative CT method at Day 15. The expression of osteogenic markers RUNX2, ALP, Collagen 1 $\alpha$ 1 (COL1 $\alpha$ 1), Osteocalcin (BGLAP), Osteonectin (SPARC), and Osteopontin (SPP1) were compared with controls. The sequence of Primers (Eurofin MSW Operon, UK) used for RT-qPCR reaction are depicted in supplementary information (Table S4).

## 2.3 | Ectopic bone formation

All in vivo experiments were performed under the permission from Danish National Ethical committee on animal experiments. Danish regulations for care and use of laboratory animals were maintained throughout the experiments. Ectopic bone formations on cell seeded scaffolds were tested by implantation of cell laden scaffolds subcutaneously in NOD.CB17-Prkdc<sup>scid</sup>/J mice as per our lab protocol (Abdallah, Ditzel, & Kassem, 2008).  $5 \times 10^5$  cells were seeded on scaffolds in vitro and were implanted subcutaneously. Each mouse had four implants, two were the cell laden PVA-PCL-HABs and other two implants were cells seeded on 40 mg hydroxyapatite-tricalcium phosphate (HA/TCP, Triosite 0.5–1 mm granules, Biomatlante/Zimmer, Vigneux de Bretagne, France), which served as the control (Harkness et al., 2011). DPSC ( $n = 4$ ) and hMSC ( $n = 4$ ) seeded scaffolds were used in separate mice. 8 weeks after implantation, the scaffolds and implants were removed and fixed in 4% paraformaldehyde and decalcified with 0.38 M EDTA before embedding in paraffin. Sections were stained with haematoxylin and eosin, human

Vimentin antibody (clone SP20, Thermo Scientific), and Collagen Type I antibody (Col Type I; LF-67 kindly provided by Dr. Larry Fisher, the National Institute of Dental and Craniofacial Research, National Institutes of Health) and Sirius red in picric acid (Sirius red F3BA), imaged under polarized light.

### 2.3.1 | Statistical analysis

All in vitro experiments were performed in at least in triplicates. The data represented are mean  $\pm$  standard error of the mean. The comparisons between groups were carried out by analysis of variance with multiple comparisons followed by Tukey post hoc test. t-Tests were performed when only two groups were compared. Statistical analysis was performed using GraphPad Prism (version 6.00, GraphPad Software, La Jolla California USA).  $p$  Values  $<.05$  were considered significant.

## 3 | RESULTS

### 3.1 | Physicochemical characterization of PVA-PCL-HAB scaffold

The PVA-PCL-HAB was fabricated using the electrospinning process with dual pump and dual syringe. (Figure 1a), shows fibre morphology visualized by SEM. The fibres are smooth, randomly aligned, and formed a sheet consisting of interpenetrating network of thick ( $1,000 \pm 240$  nm;  $n = 60$ ) and thin fibres ( $230 \pm 100$  nm;  $n = 60$ ). The pores in range from 2–20  $\mu$ m, were measured from SEM images. The bioceramic HAB particles dispersed in PCL solution during scaffold manufacturing adhere to the thick fibres with visible granules (Figure 1a).

The IR spectra (Figure 1b) exhibited characteristic peaks of individual polymers PVA and PCL as well as pure HAB and PVA-PCL-HAB. The spectra of pure polymer PCL show characteristic IR bands (Table S2) of  $1,721$   $\text{cm}^{-1}$  attributed to C=O stretching (str), and C-O str bands at  $1,238$  and  $1,292$   $\text{cm}^{-1}$ . C-O-C str frequencies of  $1,164$ ,  $1,108$ , and  $1,049$  and the  $2,941$   $\text{cm}^{-1}$  are attributed to the asymmetric (Asy.str) of CH<sub>2</sub> bands. All the typical bands for PCL were also seen in PVA-PCL-HAB. Characteristic broad peaks at  $3,259$   $\text{cm}^{-1}$  attributed to OH str and CH<sub>2</sub> vibration (Vib) band at  $1,417$   $\text{cm}^{-1}$  were seen in both pure PVA and PVA-PCL-HAB. Characteristic  $1,050$   $\text{cm}^{-1}$  peak attributed to Si-O-Si strand  $960$ ,  $934$ ,  $583$ , and  $546$   $\text{cm}^{-1}$  peaks, attributed to PO<sub>4</sub><sup>3-</sup> ions were observable in pure HAB and PVA-PCL-HAB. These data confirms that all polymers and bioceramic particles are present in the material.

Thermal stability was assessed by TGA studies. TGA thermogram of electrospun PVA, PCL, and the PVA-PCL-HAB scaffolds shows that the materials are thermally stable at 37 °C (Figure 1e), and the thermogram of PVA showed the onset of decomposition at about 60 °C caused by the loss of water present in the scaffold. The second decomposition demonstrates breaking up of C-H bonds. The temperature at which 50% of the mass loss occurs is generally considered as a measure of thermal stability. In the case of PVA, 50% mass is remaining at 299 °C and 7.34% mass is remaining at 494 °C. PCL has good thermal stability with onset of decomposition near to 330 °C, and mass loss was less than 8% even at 353 °C. Half of mass



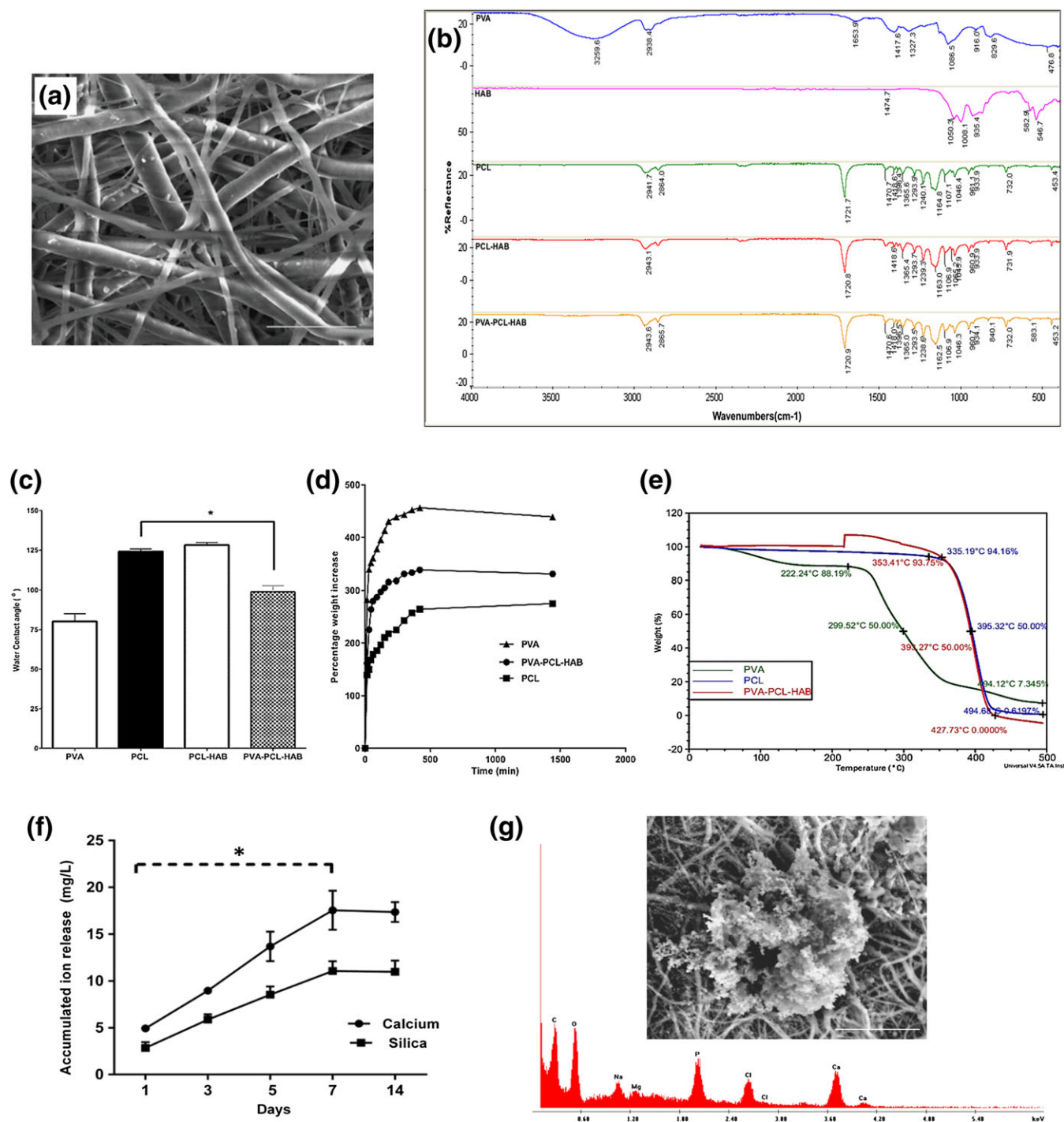


**FIGURE 1** Physicochemical characterization. (a) Scanning electron microscopic (SEM) image PVA-PCL-HAB (scale bar: 5  $\mu\text{m}$ ). (b) Stacked FTIR spectra shows peaks of PVA, HAB, PCL, PCL-HAB, and PVA-PCL-HAB. (c) Water contact angle measurement of PVA, PCL, PCL-HAB, and PVA-PCL-HAB. (\**p* < .05), (d) swelling profile of PCL, PVA-PCL-HAB, and PCL (e) thermogram of PVA, PCL, and PVA-PCL-HAB. (f) ICP-OES analyses of ion washout PVA-PCL-HAB. (\**p* < .05). (g) SEM (scale bar: 50  $\mu\text{m}$ ) and electron dispersive X-ray spectra show apatite crystals formation at Day 30 after immersion in stimulated body fluid; HAB = hydroxyapatite based bioceramic; PVA = polyvinyl alcohol; PCL = poly ( $\epsilon$ ) caprolactone; FTIR = Fourier transform infrared; ICP = inductive coupled plasma; OES = optical emission spectroscopy

is remaining at 395 °C and 0.6% mass only is remaining at 494 °C. The thermal stability of PCL is significantly greater than that of PVA. The thermal degradation pattern of the hybrid scaffold PVA-PCL-HAB tended to become similar to PCL. The hybrid material thus has a very good thermal stability with 50% mass loss at a slightly elevated temperature of 398 °C.

The hydrophilicities of the materials were assessed by studying their water absorption capacity and their air-water contact angles. Water contact angle measurements of PVA scaffolds and PCL scaffolds were ( $80.27^\circ \pm 11.8$ ) and ( $124^\circ \pm 3.7$ ), respectively (Figure 1c). The combination of PVA fibres and PCL fibres showed significant increase in hydrophilic affinity ( $98.85^\circ \pm 9.6$ ; *p* < .05) of

PVA-PCL-HAB, when compared with PCL scaffold. PCL is hydrophobic, and its swelling index at pH 7.4 was around 260%. PVA on the other hand has been reported to be hydrophilic, and we observed a higher swelling of around 450%. Coelectrospinning PCL and the hydrophilic PVA increased the hydrophilicity and water absorption capacity of the hybrid material. As shown in (Figure 1d), the water absorption capacity estimated by swelling of the hybrid material is around 350% that lies between the values observed for the individual polymers. Thus, the swelling studies ensure that the hydrophilic/hydrophobic tuning can be achieved by appropriate coelectrospun blends of materials. Incorporation of silica particles has been reported to reduce hydrophobicity of PCL (Lee et al., 2010). Water contact angle measurements for surface hydroaffinity properties showed that the PVA-PCL-HAB scaffold had a mean contact angle significantly reduced compared with electrospun PCL under similar testing conditions. Our results indicated there is no significant change in water contact angle measurement following addition of HAB to PCL. The swelling ratio

analysis showed the swelling capacity of PVA-PCL-HAB was at an intermittent percentage of 350% between the higher swelling ratio of PVA and lower swelling ratio of PCL. The higher swelling ratio favors the perfusion of nutrients required for cell growth (Shanmugasundaram et al., 2001). The increased swelling ratio would also facilitate free ionic exchange from the scaffold.

Inductive coupled plasma optical emission spectroscopy analysis of the washout collected showed significant gradient increase in cumulative ion release of calcium and silica from the PVA-PCL-HAB until a plateau was reached at Day 7 (Figure 1f). The ion release profile also indicates that PVA-PCL-HAB was able to deliver calcium and silica ions essential for the initiation of bioactive response.

### 3.2 | SBF immersion

The apatite depositions on the biomaterial surfaces upon immersion in SBF were reported to be predictive for in vivo bone bonding ability.

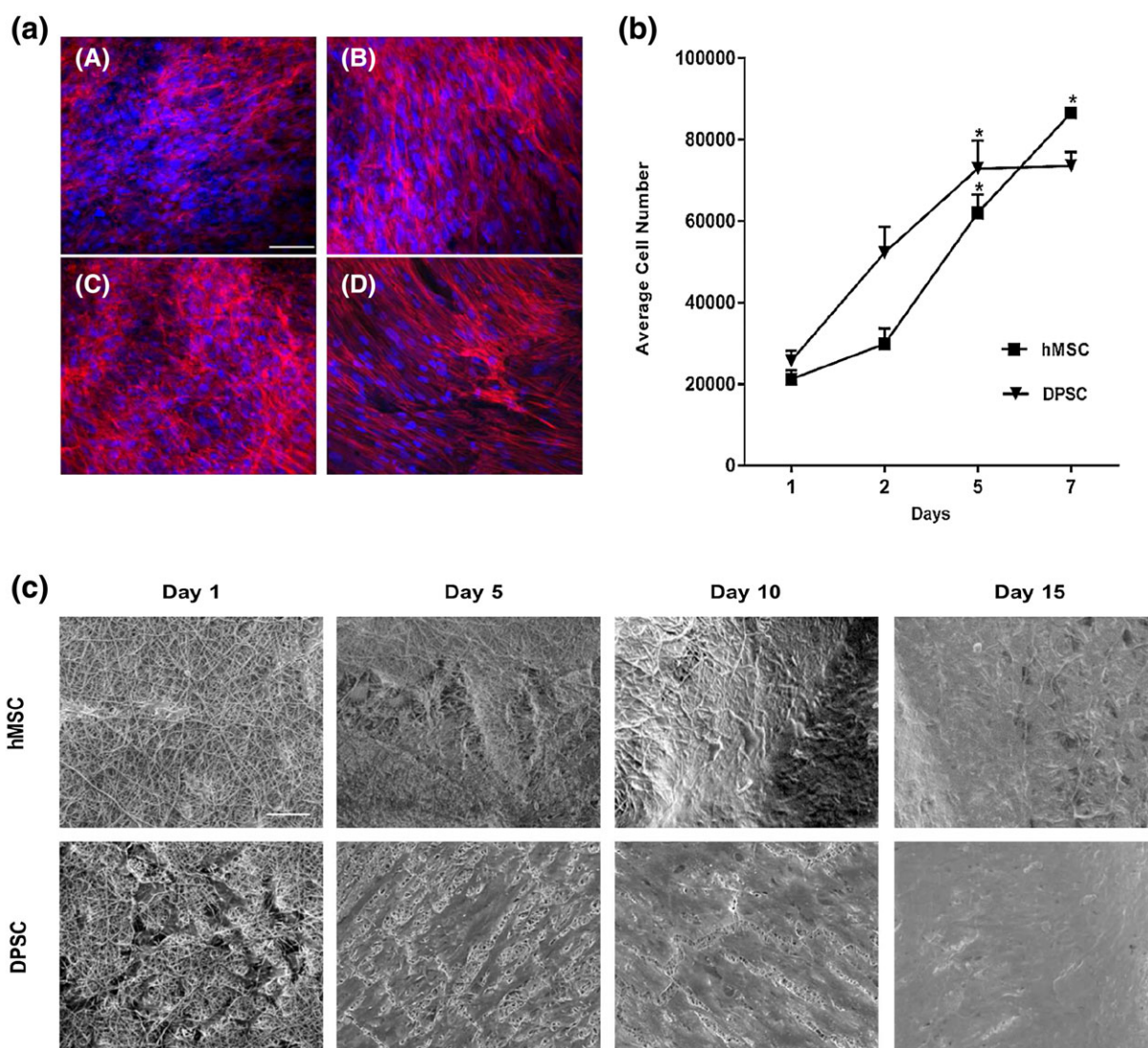


**FIGURE 2** Cell attachment, proliferation, and spreading. (a) Dapi/Phalloidin staining. Confocal microscopy of Dapi/Phalloidin stained cells attached on PVA-PCL-HAB (scale bar: 100  $\mu$ m): (A) hMSC Day 1 (B) hMSC Day 7 (C) DPSC Day 1 (D) DPSC Day 7. (b) Cell proliferation assay. A significant increase ( $*p < .05$ ) in cell number was detected for both hMSC and DPSC on PVA-PCL-HAB. (c) Cell proliferation and spreading on PVA-PCL-HAB. Scanning electron microscopy (scale bar: 50  $\mu$ m); HAB = hydroxyapatite based bioceramic; PVA = polyvinyl alcohol; PCL = poly ( $\epsilon$ ) caprolactone; hMSC = human bone marrow skeletal (mesenchymal) stem cells; DPSC = dental pulp stem cells

The SEM image of PVA-PCL-HAB samples immersed in SBF for 30 days showed accumulation of apatite like crystals (Figure 1g). The EDAX analysis of the crystals confirmed apatite deposition with peaks of calcium and phosphorous (Figure 1g).

### 3.3 | Cell characterization

Both hMSC and DPSC exhibited similar stromal cell-like morphology (Figure S1). Flow cytometry analysis showed that both hMSC and DPSC

express characteristics MSC surface markers: CD44<sup>+</sup>, CD73<sup>+</sup>, CD90<sup>+</sup>, CD105<sup>+</sup>, and CD166<sup>+</sup> and CD14<sup>-</sup> (Figure S1). hMSC cultures contained increased numbers of CD63<sup>+</sup> and CD146<sup>+</sup> cells as compared with DPSC. DPSC had a mixed CD146 positive phenotype

### 3.4 | Cell viability, proliferation, and spreading

DAPI and Phalloidin staining at day one postcell seeding on PVA-PCL-HAB; (Figure 2a) revealed good cell attachment as evidenced

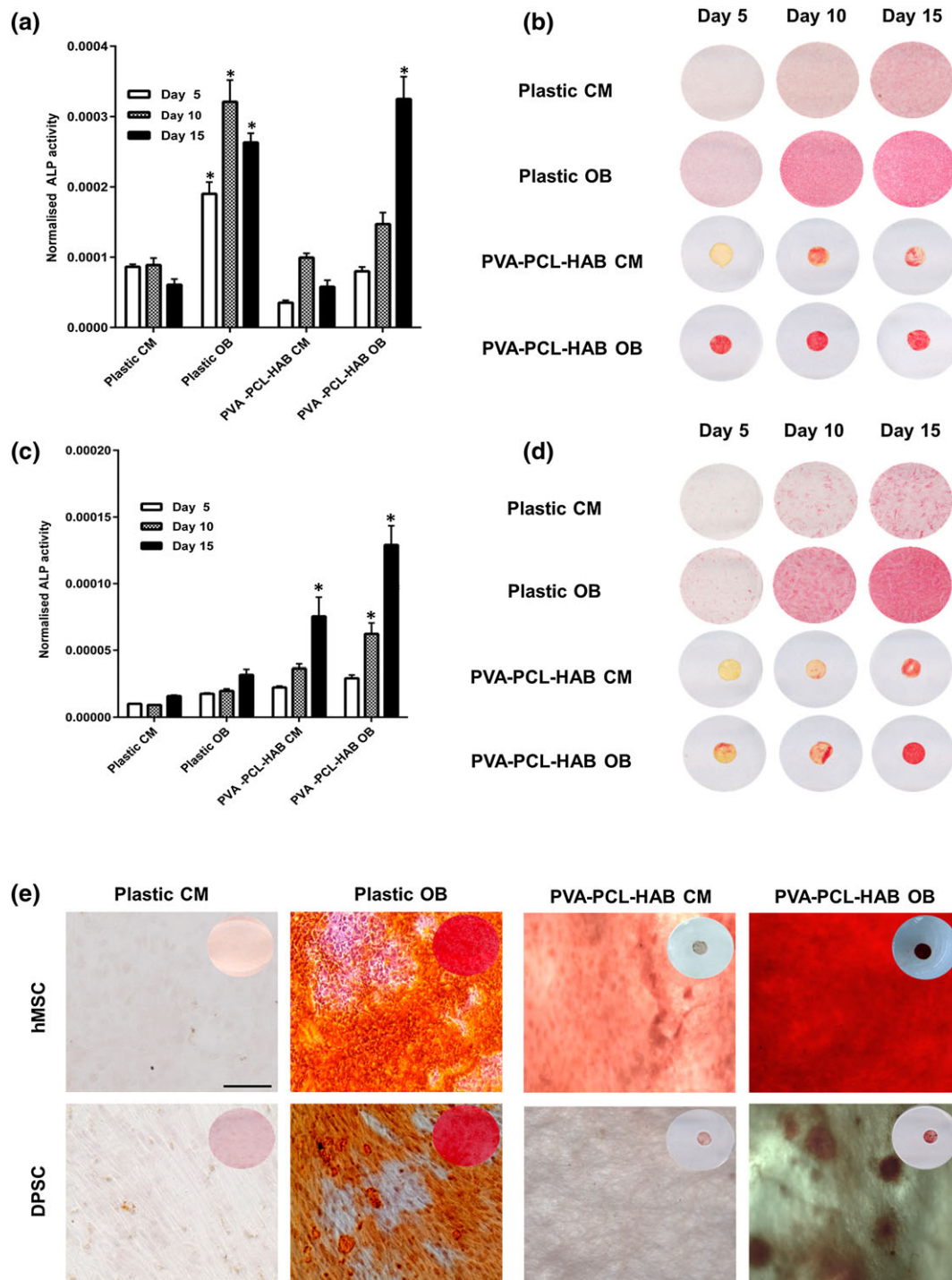


**FIGURE 3** Osteoblastic differentiation and mineralization. (a) ALP activity hMSC (\* $p < .05$ ), (b) ALP staining hMSC, (c) ALP activity DPSC (\* $p < .05$ ), (d) ALP staining DPSC, (e) alizarin red staining (scale bar: 200  $\mu$ m); inset shows macroscopic view; ALP = alkaline phosphatase; hMSC = human bone marrow skeletal (mesenchymal) stem cells; DPSC = dental pulp stem cells



by the presence of elongated actin filaments. By Day 7, the cells were evenly distributed throughout the scaffold. Both hMSC and DPSC proliferated efficiently on the PVA-PCL-HAB scaffold. Cell number as estimated by cell-Titre blue assay revealed increased cell number up to 7 days postseeding (Figure 2b). SEM analysis showed both hMSC and DPSC attach, proliferate, and spread on the scaffold surface (Figure 2c). Both cell types formed confluent cell sheet with only limited visible on PVA-PCL-HAB surface by Day 15.

### 3.5 | ALP activity

We employed ALP activity as a marker for osteoblastic lineage commitment. The ALP activities of both cell lines were compared when cultured on plastic surfaces and on PVA-PCL-HAB scaffold. Both cell types increased their ALP activity in response to osteoblast induction media.

However, we observed some quantitative differences in ALP activity. For hMSC, the maximal ALP activity was observed at Day 10 when cultured on plastic and on Day 15 when cultured on PVA-PCL-HAB scaffold (Figure 3a), and there was no significant difference in maximal ALP activity. For DPSC, ALP activity was low when cultured on plastics compared with PVA-PCL-HAB scaffold. Similar to hMSC, maximal ALP activity was observed on Day 15 when cultured on PVA-PCL-HAB scaffold (Figure 3c). Similar results were obtained from cytochemical staining for ALP of cultured cells on plastic and on PVA-PCL-HAB scaffold (Figure 3b,d).

### 3.6 | Ex vivo mineralization

The ability of PVA-PCL-HAB scaffold to support the formation of in vitro mineralized matrix was examined. Following in vitro osteoblast differentiation induction, cells cultured on plastics and on PVA-PCL-

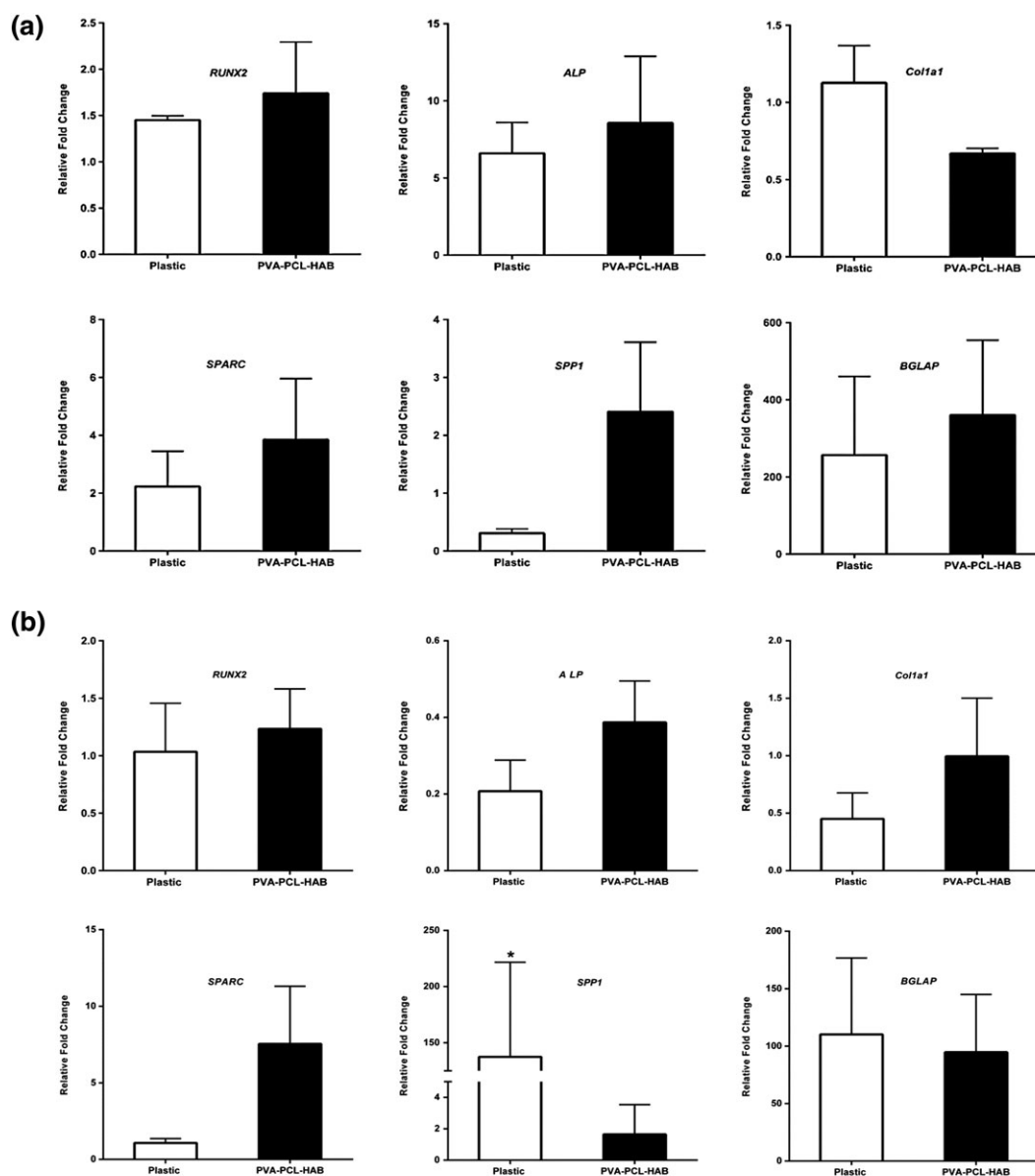


**FIGURE 4** Osteogenic gene expression relative fold change by RT-qPCR analysis at Day 15 on plastic and PVA-PCL-HAB (\* $p < .05$ ): (a) hMSC (b) DPSC; HAB = hydroxyapatite based bioceramic; PVA = polyvinyl alcohol; PCL = poly ( $\epsilon$ ) caprolactone; hMSC = human bone marrow skeletal (mesenchymal) stem cells; DPSC = dental pulp stem cells; ALP = alkaline phosphatase



HAB scaffold were examined for the presence of mineralized matrix as visualized by AZR staining. Both cell types formed mineralized matrix at Day 15 postosteoblast differentiation, when cultured on plastics (Figure 3e), and similar pattern was observed on PVA-PCL-HAB scaffold. However, hMSC exhibited more intense staining (Figure 3e).

### 3.7 | Ex vivo osteoblastic gene expression

We also examined for the ability of PVA-PCL-HAB scaffold to maintain the differentiated osteoblastic phenotype compared with standard

plastic culture surfaces. The expressions of RUNX2, Col1a1, ALP, SPARC, SPP1, and BGLAP, mRNA were quantitated at Day 15 following in vitro osteoblast differentiation induction (Figure 4). Both hMSC and DPSC expressed osteoblast gene markers when cultured on plastic and on PVA-PCL-HAB scaffold (Figure 4). However, some markers exhibited quantitative differences when the cells were cultured on plastic versus PVA-PCL-HAB scaffold. For hMSC (Figure 4a), Col1a1 expression was higher when cells cultured on plastics, whereas SPP1 was higher when cells were cultured on PVA-PCL-HAB scaffold. Similarly, DPSC exhibited a dramatic upregulation expression of SPP1

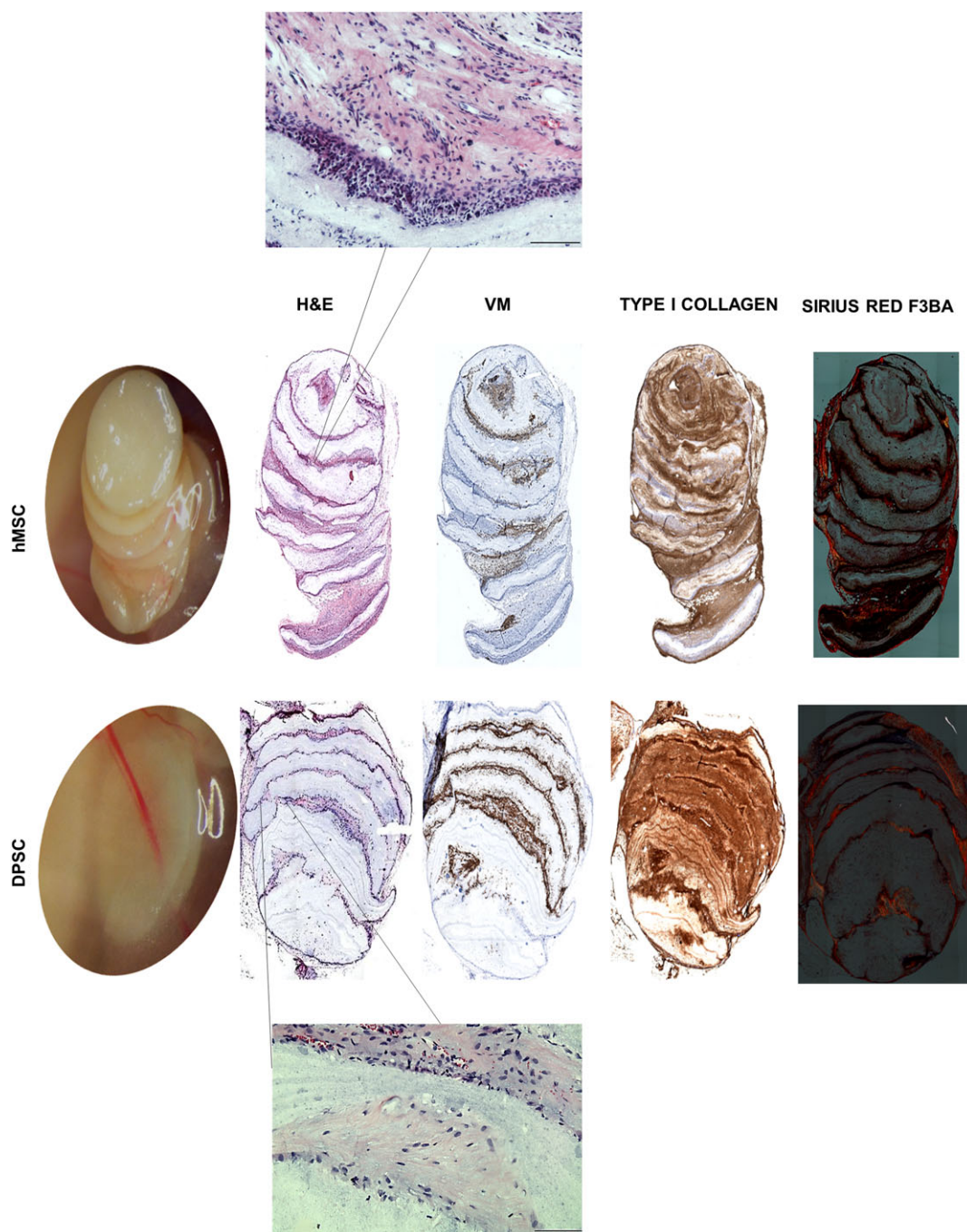


**FIGURE 5** In vivo implantations in NOD-SCID mice. At 8 weeks, ectopic bone formation on subcutaneous implantation demonstrate blood vessel ingrowth seen both cell groups (hMSC and DPSC). Histology mosaic image (10 $\times$ ) magnification and the inset (H & E) shows bone formation and cell migration through PVA-PCL-HAB. Human antivimentin (VM) stain shows presence of cells of human origin; HAB = hydroxyapatite based bioceramic; PVA = polyvinyl alcohol; PCL = poly ( $\epsilon$ ) caprolactone; hMSC = human bone marrow skeletal (mesenchymal) stem cells; DPSC = dental pulp stem cells

when cultured on plastic compared with cells cultured on PVA-PCL-HAB scaffold (Figure 4b).

### 3.8 | In vivo ectopic bone formation

All mice implanted with PVA-PCL-HAB scaffolds were healthy, gained weight, and had no signs of inflammation during the experiment. 8 weeks postsubcutaneous implantation in immune deficient mice; PVA-PCL-HAB implants were vascularized as seen by visual inspection (Figure 5 and inset). Histologic examination (Figure 5) showed areas of bone formation in implants containing either hMSC or DPSCs as evidenced by the presence of a positive stain of Type I collagen and the presence of characteristics birefringence of organized collagen Type I (Sirius Red F3BA). These matrixes were produced by the cells of human origin, as evidenced by positive staining of human specific anti-Vimentin antibody (Figure 5).

## 4 | DISCUSSION

The aim of the present study was to develop a biodegradable and less invasive electrospun biomaterial that supports skeletal stem cell osteoblastic differentiation and bone formation with vascularization in the peripheral and craniofacial skeleton. In the present study, we have demonstrated that an electrospun PVA-PCL-HAB scaffold can support osteoblast differentiation of two types of stem cells relevant to bone tissue regeneration: bone marrow derived skeletal stem cells and DPSC as well as in vivo ectopic bone model.

We fabricated an electrospun scaffold with nano-fibrous porous structure to mimic the native extracellular matrix of bone (Holzwarth & Ma, 2011; Wang, Ding, & Li, 2013). The PVA-PCL-HAB scaffold composes a dual electrospun network of PCL and PVA that has incorporated HAB bioceramic to facilitate osteoconductivity. Hydrophilic PVA is included in the scaffold as it degrades faster than PCL, and thus, reducing the bulk of the scaffold as new bone is formed. The combination of PVA and PCL is used for enhancing the hydrophilicity; cell attachment allows better cell penetration upon attachment. We have also included in the scaffold a bioceramic: HAB. Bioceramics support bone formation by hydroxycarbonate apatite (HCA; Hench & Paschall, 1973). The HAB used for scaffold fabrication was a triphasic bioceramic (an amorphous mixture of hydroxyl apatite, beta TCP and calcium silicate, and traces of magnesium). The optimized concentration of magnesium was added to improve sintering window without affecting bioactivity (Ma, Chen, Wang, Jiao, & Shi, 2010). The incorporation of magnesium along with beta TCP has been reported to generate an osteoimmunomodulatory effect and inhibit osteoclastogenesis (Chen et al., 2014).

We mixed HAB with PCL before electrospinning to produce electrospun PVA-PCL-HAB composite. The anticipated bioactive mechanism is based on HAB releasing calcium and phosphate ions upon contact with body fluids that raise local pH and form a silica rich interface as well as facilitating surface mobilization and accumulation of amorphous apatitic calcium phosphate phase. Assimilation of hydroxyls and carbonates from the solution by the apatitic calcium phosphate phase leads to reorganization and deposition of HCA. The HCA layer binds to the host bone by its interaction with collagen fibrils of the native bone. We employed a number of technologies to

confirm the expected biophysical characteristics of PVA-PCL-HAB scaffold. The SEM images confirmed that the electrospinning of PVA-PCL-HAB resulted in nano-fibrous porous network. The presence of bioceramic granules on the thick fibres denote that thick fibres were PCL and the EDAX spectra of the granules also confirmed the elemental peaks of calcium, phosphate, silica, and magnesium. The FTIR spectral peaks confirm the presence of PCL, PVA, and HAB in the electrospun scaffold. The thermal stability data confirmed the stability of the PVA-PCL-HAB was comparable to highly stable PCL, and the thermal stability was also considerably higher than PVA. The PVA-PCL-HAB scaffold depicted the typical characteristic peaks of all the constituent individual materials with no evidence of covalent interactions. Hence, the composite material maintains the characteristics of the constituent materials and act as a synergistic blend (Mohan & Nair, 2008).

Ion washout release profile studies demonstrated that calcium and silica ions were released from PVA-PCL-HAB scaffold. The release of calcium and silicon increased until Day 7, where it attained a plateau. The lower levels of released silicon ions when compared with calcium ions released were proportional to the lower percentage of silicates incorporated while fabrication of HAB. Silicon ions are only required for initiation of bioactive reaction, whereas the progression of reaction and completion of the reaction would be governed by calcium and phosphate complex (Hench, 1991)

We tested the hypothesized bioactivity and bone bonding of the scaffold by SBF immersion experiments in accordance with the proposal by Kokubo and Takadama that any bone bonding surface is expected to produce apatite like structure upon immersion in SBF for a period of 4 weeks (Kokubo & Takadama, 2006). SEM images of the SBF immersed PVA-PCL-HAB showed surface deposition of apatite like crystals at Day 30. The EDS examination of crystals showed increased calcium and phosphate peaks indicative of apatite crystal formation.

We tested two stromal derived stem cells: DPSC and hMSC. DPSC are stem cells of neural crest origin (Arthur, Rychkov, Shi, Koblar, & Gronthos, 2008; La Noce et al., 2014), whereas hMSC are bone marrow derived skeletal stem cells of mesodermal origin; both the stem cells are capable of bone formation in craniofacial region (Tollemar, Collier et al., La Noce et al., 2014, Tollemar et al., 2016). Generally, both cell types exhibited similar phenotype but we observed some quantitative differences. Fewer CD146 expressing cells were present in DPSC cultures compared with bone marrow hMSC. CD146 expressions have been reported to associated with osteogenic potential of bone marrow hMSC (Sacchetti et al., 2007).

We observed that both hMSC and DPSC attached readily to the PVA-PCL-HAB scaffold and more than 70% of the seeded cells attached at Day 1 postseeding. Cell attachment on the scaffold surface is dependent on the method of seeding and hydroaffinity of the scaffold surface. We employed the sessile drop high density seeding method that has been reported to provide maximal cell attachment (Reynolds, Riehle, & Gadegaard, 2014).

PVA-PCL-HAB scaffold with its balanced hydrophobic-hydrophilic properties supported cell viability and proliferation of both bone marrow hMSC and DPSC. Both cell types were seen to be uniformly distributed, viable, and proliferating on the scaffold. However, the

three dimensional distribution of the cells in the scaffold 3D architecture impedes its quantification. Hence, we adopted the cell titre blue assay to quantify the average number of viable cells present at different time points. The hMSC were seen to proliferate at significantly higher rate at Day 7 when compared with DPSC that continued at stationary phase.

The ability of PVA-PCL-HAB scaffold to support osteoblastic differentiation of hMSC and DPSC cells were tested using a number of criteria: ALP activity, osteoblastic gene expression, and the ability to form mineralized matrix. Although we observed similar results between hMSC and DPSC, there were quantitative differences in the levels of ALP activity or osteoblastic gene expression that can be explained by differences in cell confluence and cell number as these factors may exert additional effects independent of the differentiated status of the cells (Tomlinson, Dennis, Yang, & Kirkham, 2015). In addition to the ability of PVA-PCL-HAB scaffold to support in vitro osteoblast differentiation of DPSC and hMSC, it supported bone formation in vivo in an ectopic bone formation model. We observed good vascularization of the PVA-PCL-HAB scaffold that may be linked to stimulated local production of vascular endothelial growth factor by the dissolute products of HAB (Day et al., 2004). Histological analysis of the implants demonstrates the ability of the PVA-PCL-HAB scaffold to support bone formation. The in vivo implantations without inducing the seeded cells also confirm the ability of scaffold to receive molecular cues from host tissue and synchronize bone formation. The material could hence be used as a soft and less invasive scaffold for bone defects of the craniofacial region.

The highlighting feature of the study was to reproduce the in vitro bone formation results in an in vivo setting even in the absence of osteogenic induction through using appropriate biomaterial of the study. These in vivo studies provide a supportive data to the first time report of potential clinical use of this scaffold in contrast to any other previously reported polymer based biomaterials.

## 5 | CONCLUSIONS

In this study, we have developed an electrospun PVA-PCL-HAB scaffold with a hydrophobic-hydrophilic nature and promoting osteoconductivity. The scaffold has ability to support proliferation, osteoblastic differentiation, and bone formation for two different stem cell types: hMSC and DPSC in vitro. The biomaterial further supports skeletal stem cell osteoblastic differentiation and bone formation with vascularization in vivo. These results encourage testing of this material for therapeutic applications of bone regeneration in the field of orthopedics and dentistry. Hence, we recommend PVA-PCL-HAB scaffold with multiple applications as an ideal material for vascularized craniofacial bone tissue engineering. Further studies with craniofacial defects in mice and large animal models are planned in the future.

## ACKNOWLEDGEMENTS

Authors would like to acknowledge Nicholas Ditzel for help with implantation studies, Lone Christiansen, for technical assistance with

histological processing of the implants. We thank Lisbeth A. Abildtrup, Aarhus Dental School for isolation of DPSC, Ulla Melchior Hansen, Danish Molecular Biomedical Imaging Center for assistance in confocal imaging, and Dr S. Suresh Babu and Dhanesh Vaikkat from SCTIMST, India, for assistance in fabrication of scaffold. Authors also thank Nimi N, DTERT, and SCTIMST for technical assistance. The study was supported by an Indo-Danish grant obtained from the strategic research council of Denmark and Department of Biotechnology, India. This work was also supported Lund beck Foundation Nano medicine Center for Individualized Management of Tissue Damage and Regeneration. The funding bodies provided monetary support only.

## AUTHORS CONTRIBUTIONS

Concept, designing of experiments, analytical interpretation of results, and manuscript preparation: R.D.P., D.C.K., B.M., H.K.V., P.D.N., J.K., and M.K. Cell characterizations and experiment protocols establishment: R.D.P. & L.H. Biomaterial designing and characterization: R.D.P., H.K.V., and P.D.N.

## DISCLOSURES

No potential conflicts of interest exist.

## ORCID

Rahul Damodaran Prabha  <http://orcid.org/0000-0002-7591-9287>

## REFERENCES

- Abdallah, B. M., Ditzel, N., & Kassem, M. (2008). Assessment of bone formation capacity using in vivo transplantation assays: Procedure and tissue analysis. In J. J. Westendorf (Ed.), *Osteoporosis: Methods and protocols* (pp. 89–100). Totowa, NJ: Humana Press.
- Al-Nbaheen, M., Vishnubalaji, R., Ali, D., Bouslimi, A., Al-Jassir, F., Megges, M., ... Aldahmash, A. (2013). Human stromal (mesenchymal) stem cells from bone marrow, adipose tissue and skin exhibit differences in molecular phenotype and differentiation potential. *Stem Cell Reviews*, 9(1), 32–43.
- Andersen, O. Z., Offermanns, V., Sillassen, M., Almtoft, K. P., Andersen, I. H., Sorensen, S., ... Foss, M. (2013). Accelerated bone ingrowth by local delivery of strontium from surface functionalized titanium implants. *Biomaterials*, 34(24), 5883–5890.
- Arthur, A., Rychkov, G., Shi, S., Koblar, S. A., & Gronthos, S. (2008). Adult human dental pulp stem cells differentiate toward functionally active neurons under appropriate environmental cues. *Stem Cells*, 26(7), 1787–1795.
- Chen, Z., Mao, X., Tan, L., Friis, T., Wu, C., Crawford, R., & Xiao, Y. (2014). Osteoimmunomodulatory properties of magnesium scaffolds coated with beta-tricalcium phosphate. *Biomaterials*, 35(30), 8553–8565.
- Ciapetti, G., Ambrosio, L., Savarino, L., Granchi, D., Cenni, E., Baldini, N., ... Giunti, A. (2003). Osteoblast growth and function in porous poly epsilon-caprolactone matrices for bone repair: A preliminary study. *Biomaterials*, 24(21), 3815–3824.
- Day, R. M., Boccaccini, A. R., Shurey, S., Roether, J. A., Forbes, A., Hench, L. L., & Gabe, S. M. (2004). Assessment of polyglycolic acid mesh and bioactive glass for soft-tissue engineering scaffolds. *Biomaterials*, 25(27), 5857–5866.
- García, J., & García, A. (2015). Biomaterial-mediated strategies targeting vascularization for bone repair. *Drug Delivery and Translational Research*: 1–19.
- Giannoudis, P. V., Dinopoulos, H., & Tsiridis, E. (2005). "Bone substitutes: An update." *Injury* 36(3, Supplement): S20-S27.



- Gorustovich, A. A., Roether, J. A., & Boccaccini, A. R. (2010). Effect of bioactive glasses on angiogenesis: A review of in vitro and in vivo evidences. *Tissue Engineering. Part B, Reviews*, 16(2), 199–207.
- Harkness, L., Mahmood, A., Ditzel, N., Abdallah, B. M., Nygaard, J. V., & Kassem, M. (2011). Selective isolation and differentiation of a stromal population of human embryonic stem cells with osteogenic potential. *Bone*, 48(2), 231–241.
- Hench, L. L. (1991). Bioceramics: From concept to clinic. *Journal of the American Ceramic Society*, 74(7), 1487–1510.
- Hench, L. L., & Paschall, H. A. (1973). Direct chemical bond of bioactive glass-ceramic materials to bone and muscle. *Journal of Biomedical Materials Research*, 7(3), 25–42.
- Holzwarth, J. M., & Ma, P. X. (2011). Biomimetic nanofibrous scaffolds for bone tissue engineering. *Biomaterials*, 32(36), 9622–9629.
- Jones, J. R. (2013). Review of bioactive glass: From hench to hybrids. *Acta Biomaterialia*, 9(1), 4457–4486.
- Kokubo, T., & Takadama, H. (2006). How useful is SBF in predicting in vivo bone bioactivity? *Biomaterials*, 27(15), 2907–2915.
- Kouroupis, D., Baboolal, T. G., Jones, E., & Giannoudis, P. V. (2013). Native multipotential stromal cell colonization and graft expander potential of a bovine natural bone scaffold. *Journal of Orthopaedic Research*, 31(12), 1950–1958.
- Kraft, D. C., Bindslev, D. A., Melsen, B., Abdallah, B. M., Kassem, M., & Klein-Nulend, J. (2010). Mechanosensitivity of dental pulp stem cells is related to their osteogenic maturity. *European Journal of Oral Sciences*, 118(1), 29–38.
- La Noce, M., Mele, L., Tirino, V., Paino, F., De Rosa, A., Naddeo, P., ... Desiderio, V. (2014). Neural crest stem cell population in craniomaxillofacial development and tissue repair. *European Cells & Materials*, 28, 348–357.
- Lee, E. J., Teng, S. H., Jang, T. S., Wang, P., Yook, S. W., Kim, H. E., & Koh, Y. H. (2010). Nanostructured poly(epsilon-caprolactone)-silica xerogel fibrous membrane for guided bone regeneration. *Acta Biomaterialia*, 6(9), 3557–3565.
- Ma, J., Chen, C. Z., Wang, D. G., Jiao, Y., & Shi, J. Z. (2010). Effect of magnesia on the degradability and bioactivity of sol-gel derived SiO<sub>2</sub>-CaO-MgO-P<sub>2</sub>O<sub>5</sub> system glasses. *Colloids and Surfaces B: Biointerfaces*, 81(1), 87–95.
- Mikos, A. G., Herring, S. W., Ochareon, P., Elisseff, J., Lu, H. H., Kandel, R., ... Vunjak-Novakovic, G. (2006). Engineering complex tissues. *Tissue Engineering*, 12(12), 3307–3339.
- Mohan, N., & Nair, P. D. (2008). Polyvinyl alcohol-poly(caprolactone) semi IPN scaffold with implication for cartilage tissue engineering. *Journal of Biomedical Materials Research. Part B, Applied Biomaterials*, 84(2), 584–594.
- Orienti, I., Bigucci, F., Gentilomi, G., & Zecchi, V. (2001). Self-assembling poly(vinyl alcohol) derivatives, interactions with drugs and control of release. *Journal of Pharmaceutical Sciences*, 90(9), 1435–1444.
- Qiu, W., Hu, Y., Andersen, T. E., Jafari, A., Li, N., Chen, W., & Kassem, M. (2010). Tumor necrosis factor receptor superfamily member 19 (TNFRSF19) regulates differentiation fate of human mesenchymal (stromal) stem cells through canonical Wnt signaling and C/EBP. *The Journal of Biological Chemistry*, 285(19), 14438–14449.
- Rainer, A., Centola, M., Spadaccio, C., Gherardi, G., Genovese, J. A., Licocchia, S., & Trombetta, M. (2010). Comparative study of different techniques for the sterilization of poly-L-lactide electrospun microfibers: Effectiveness vs. material degradation. *The International Journal of Artificial Organs*, 33(2), 76–85.
- Reynolds, P. M., Riehle, M., & Gadegaard, N. (2014). *Cell seeding method and device*. Google: Patents.
- Sacchetti, B., Funari, A., Michienzi, S., Di Cesare, S., Piersanti, I. S., Tagliafico, E., ... Bianco, P. (2007). Self-renewing osteoprogenitors in bone marrow sinusoids can organize a hematopoietic microenvironment. *Cell*, 131(2), 324–336.
- Shabani, I., Haddadi-Asl, V., Soleimani, M., Seyedjafari, E., & Hashemi, S. M. (2014). Ion-exchange polymer nanofibers for enhanced osteogenic differentiation of stem cells and ectopic bone formation. *ACS Applied Materials & Interfaces*, 6(1), 72–82.
- Shanmugasundaram, N., Ravichandran, P., Neelakanta Reddy, P., Ramamurthy, N., Pal, S., & Panduranga Rao, K. (2001). Collagen-chitosan polymeric scaffolds for the in vitro culture of human epidermoid carcinoma cells. *Biomaterials*, 22(14), 1943–1951.
- Simonsen, J. L., Rosada, C., Serakinci, N., Justesen, J., Stenderup, K., Rattan, S. I. S., ... Kassem, M. (2002). Telomerase expression extends the proliferative life-span and maintains the osteogenic potential of human bone marrow stromal cells. *Nature Biotechnology*, 20(6), 592–596.
- Thomas, L. V., & Nair, P. D. (2011). (Citric acid-co-polycaprolactone triol) polyester: A biodegradable elastomer for soft tissue engineering. *Biomatter*, 1(1), 81–90.
- Tollema, V., Collier, Z. J., Mohammed, M. K., Lee, M. J., Ameer, G. A., & Reid, R. R. (2016). Stem cells, growth factors and scaffolds in craniofacial regenerative medicine. *Genes & Diseases*, 3(1), 56–71.
- Tomlinson, M., Dennis, C., Yang, X., & Kirkham, J. (2015). Tissue non-specific alkaline phosphatase production by human dental pulp stromal cells is enhanced by high density cell culture. *Cell and Tissue Research*, 1–12.
- Wang, X., Ding, B., & Li, B. (2013). Biomimetic electrospun nanofibrous structures for tissue engineering. *Materials Today*, 16(6), 229–241.
- Wu, C., Zhou, Y., Chang, J., & Xiao, Y. (2013). Delivery of dimethylallyl glycine in mesoporous bioactive glass scaffolds to improve angiogenesis and osteogenesis of human bone marrow stromal cells. *Acta Biomaterialia*, 9(11), 9159–9168.
- Yang, F., Wang, J., Hou, J., Guo, H., & Liu, C. (2013). Bone regeneration using cell-mediated responsive degradable PEG-based scaffolds incorporating with rhBMP-2. *Biomaterials*, 34(5), 1514–1528.
- Zhu, Y., Gao, C., Liu, X., & Shen, J. (2002). Surface modification of polycaprolactone membrane via aminolysis and biomacromolecule immobilization for promoting cytocompatibility of human endothelial cells. *Biomacromolecules*, 3(6), 1312–1319.

## SUPPORTING INFORMATION

Additional Supporting Information may be found online in the supporting information tab for this article.

**Figure S1.** MSCs in culture and surface marker expression. (Scale bar: 200 μm) (A) hMSC (B) DPSC (C)hMSC surface marker expression (D) DPSC surface marker expression.

**Table S1.** Electrospinning Parameters

**Table S2.** FTIR spectra wavelength

**Table S3.** Antibody / Isotype controls used for flow cytometry

**Table S4.** Sequence of primers used for RT- qPCR

**How to cite this article:** Prabha RD, Kraft DCE, Harkness L, et al. Bioactive nano-fibrous scaffold for vascularized craniofacial bone regeneration. *J Tissue Eng Regen Med*. 2018;12:e1537–e1548. <https://doi.org/10.1002/term.2579>